Supporting Information

Enhanced pollutant photodegradation activity of graphitic carbon nitride on via bismuth oxyhalide graphene hybridization and the mechanism study

Xinghui Liu,‡*[ab] Yang Liu,‡[ab] Xiang Guo,*[b] Bowen Tao,[b] Xu Ma,[a] Simin Cheng,[a] Ning Tian,[a] Gaihui Liu,[a] Qiao Wu,[a] Viet Q Bui,[c] Kuldeep K Saxena,[d] Sankar Ganesh Ramaraj,[e] Jianhui Liu,[f] Fuchun Zhang*[a] and Yongfa Zhu*[g]

[a] School of Physics and Electronic Information, Yan'an University, Yan'an 716000, China.

[b] Science and Technology on Aerospace Chemical Power Laboratory, Laboratory of Emergency Safety and Rescue Technology, Hubei Institute of Aerospace Chemotechnology, Xiangyang, 441003, China.

[c] Advanced Institute of Science and Technology, The University of Danang, 41 Le Duan, Danang, Vietnam.

[d] Division of Research and Development, Lovely Professional University, Phagwara, India.

[e] Department of Bioengineering, The University of Tokyo, 7-3-1 Hongo, Bunkyo-Ku, Tokyo, 113-8656, Japan.

[f] Department of Restorative Dentistry and Biomaterials Sciences, Harvard School of Dental Medicine Boston, Massachusetts United States of America; The Forsyth Institute Cambridge, Massachusetts United States of America

[g] Department of Chemistry, Beijing Key Laboratory for Analytical Methods and Instrumentation, Tsinghua University, Beijing 100084, China.

‡ These authors contributed equally to this work.

* Corresponding author

E-mail addresses:

(X. Liu) liuxinghui119@gmail.com;(X. Guo) guoxiang@casc42.cn

(F. Zhang); yadxzfc@yau.edu.cn; (Y. Zhu) zhuyf@tsinghua.edu.cn.

Transient photocurrent test

Photocatalytic activity is closely related to the transfer and separation rate of photogenerated electron-hole pairs; therefore, the carrier separation behavior is often investigated through the transient photocurrent measurement. To explore the photocurrents of the four samples, the electrochemical measurements were performed with an electrochemical workstation using a four-electrode system at room temperature under simulated sunlight glowed from a 500 W Xe lamp.

Band scheme confirmation

band gap energies (E_g) about pure CN and BOB were calculated according to the following Kubelka- Munk formula:

$$\alpha hv = A(hv - E_g)^{1/2}$$

(Equation S1)

where a, h, v and A are the absorption coefficient, Planck's constant, the optical coefficient frequency and the proportionality constant[1-3].

The proposed reaction pathway for CN-BOB.

CN OR BOB +hν → e^- (CN OR BOB) + h^+ (CN OR BOB) (Equation S7)

e^- (BOB) + h^+ (CN) → Recombination (Equation S8)

$e^- + O^2 \rightarrow \cdot O_2^-$ (Equation S9)

$h^+ + OH^- \rightarrow \cdot OH$ (Equation S10)

$\cdot O_2^-$ + RhB → Degraded products (Equation S11)

h^+ + RhB → Degraded products (Equation S12)

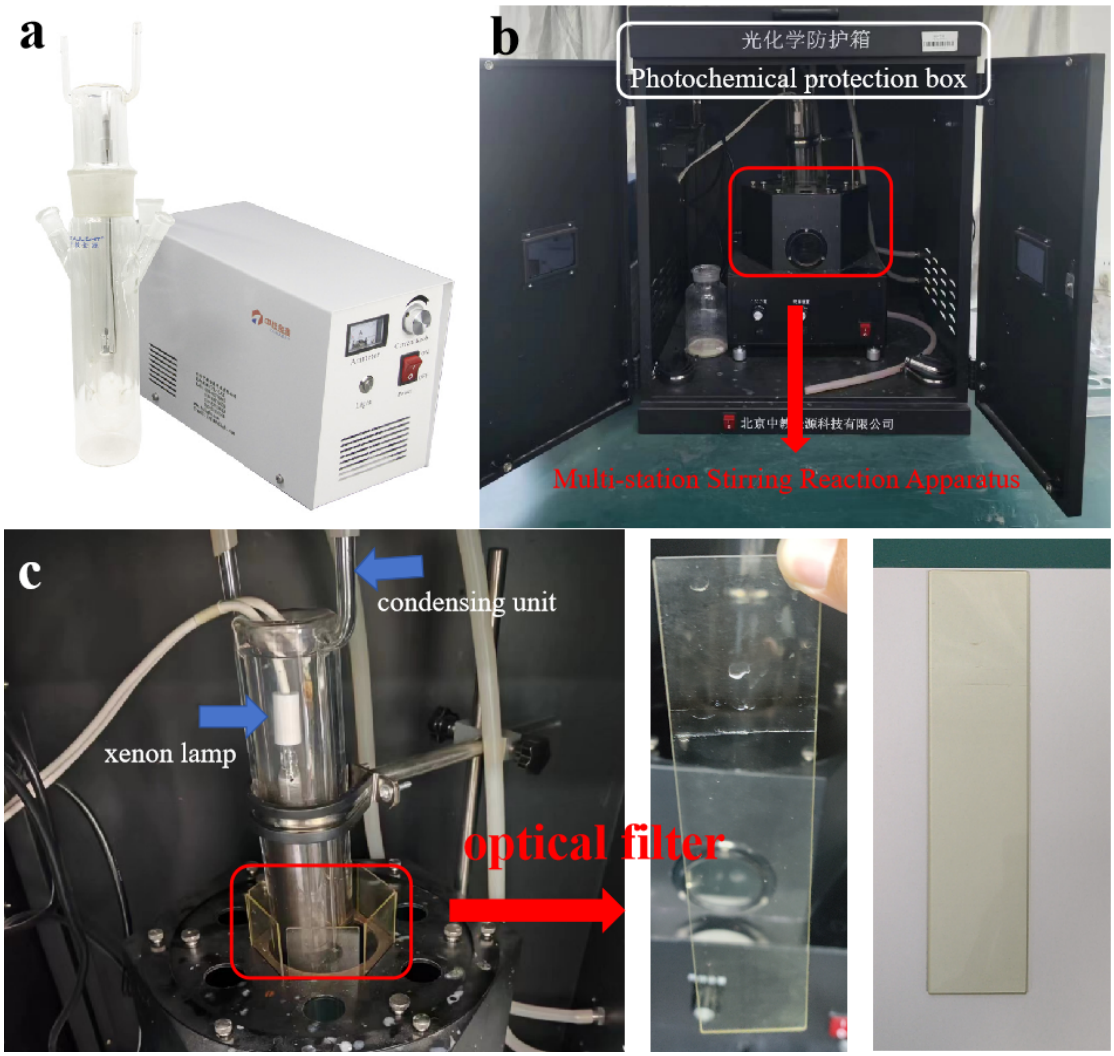

Fig. S1 (a) a is the CEL-LAX500 long arc xenon lamp, (b) the photocatalytic reaction device, and (c) a partial enlargement of the photocatalytic reaction dark box & visible light filter.

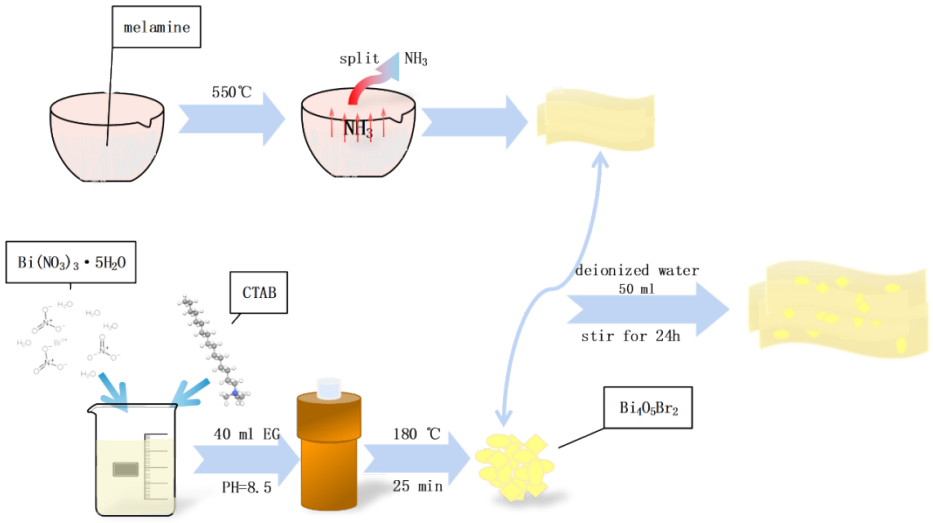

Fig. S2. synthesis procedure of g-C_3N_4/$Bi_4O_5Br_2$.

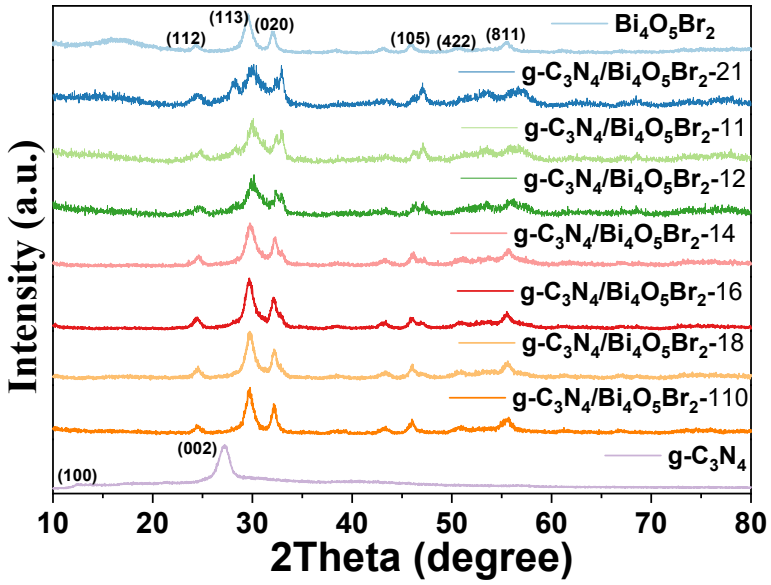

Fig. S3. XRD patterns for g-C_3N_4, $Bi_4O_5Br_2$, and various g-C_3N_4/$Bi_4O_5Br_2$-XY.

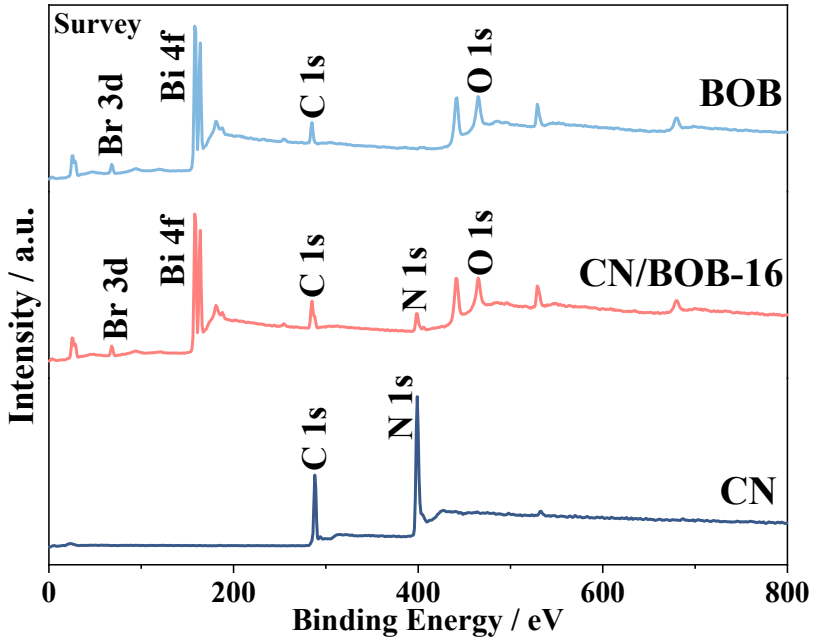

Fig. S4. XPS spectra survey.

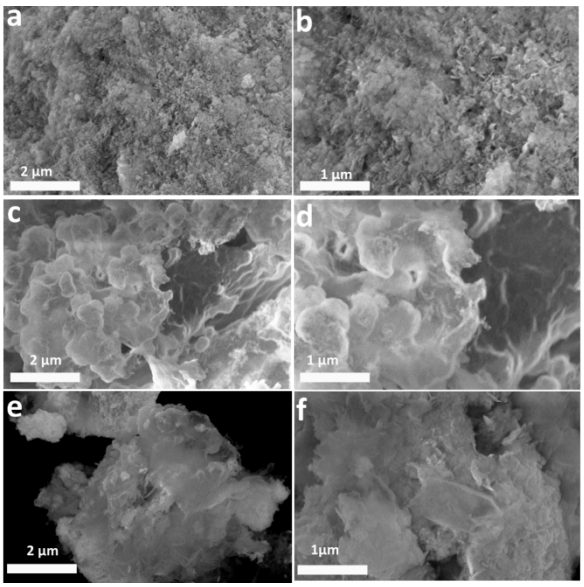

Fig. S5. SEM images. (a, b) $Bi_4O_5Br_2$, (c, d) g-C_3N_4, (e, f) CN/BOB-16 heterojunction.

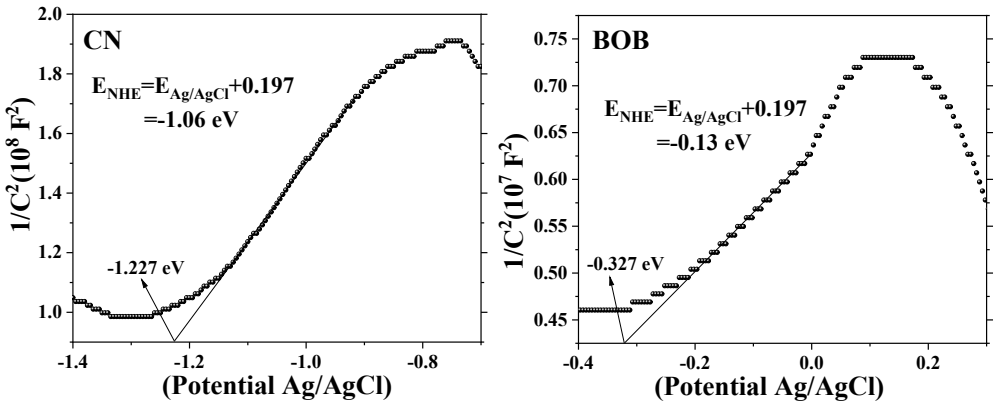

Fig. S6. Mott-Schottky curves of CN and BOB. Electrolyte properties: Na_2SO_4. The working electrode was prepared by dip-coating a photocatalyst slurry on an ITO glass electrode (2.0 × 4.0 cm2). Mott-Schottky plots were collected at a scan rate of 5 mV s-1. The counter electrode was an Ag/AgCl electrode, and the results and calculated equations after converting it to NHE are shown in Figure.

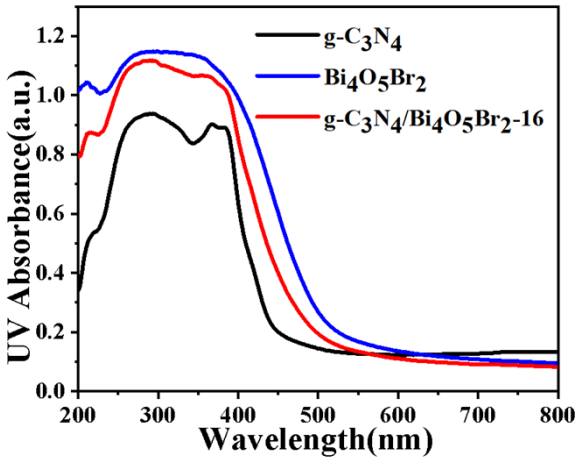

Fig. S7. UV-Vis DRS spectra.

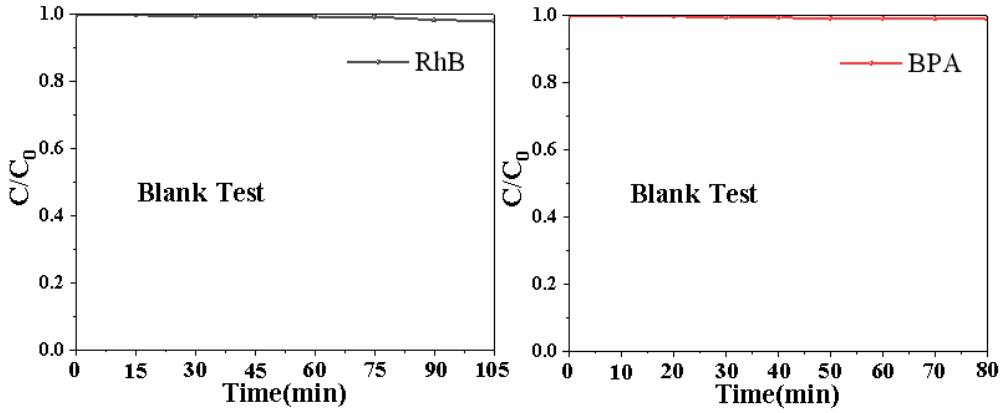

Fig. S8. The blank test with the light only.

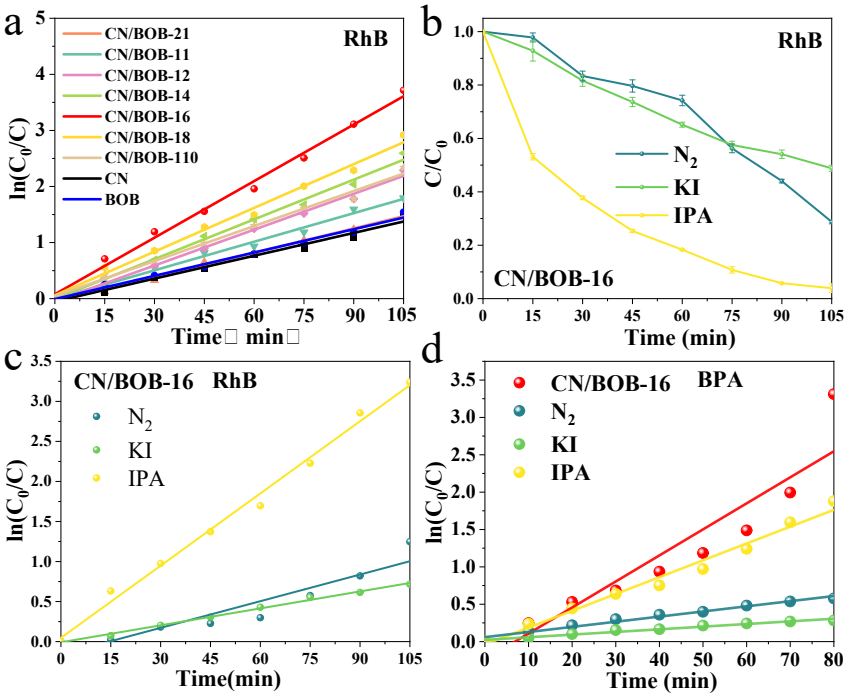

Fig. S9. (a) Pseudo-first-order kinetic curve of CN, BOB, CN/BOB-21, CN/BOB-11, CN/BOB-12, CN/BOB-14, CN/BOB-16, CN/BOB-18 and CN/BOB-110. **(b)** Assessment of active species through free radical scavenging degradation experiments. **(c)** Pseudo-primary kinetic profile of RhB degradation by CN/BOB-16. **(d)** Pseudo-primary kinetic profile of BPA degradation by CN/BOB-16.

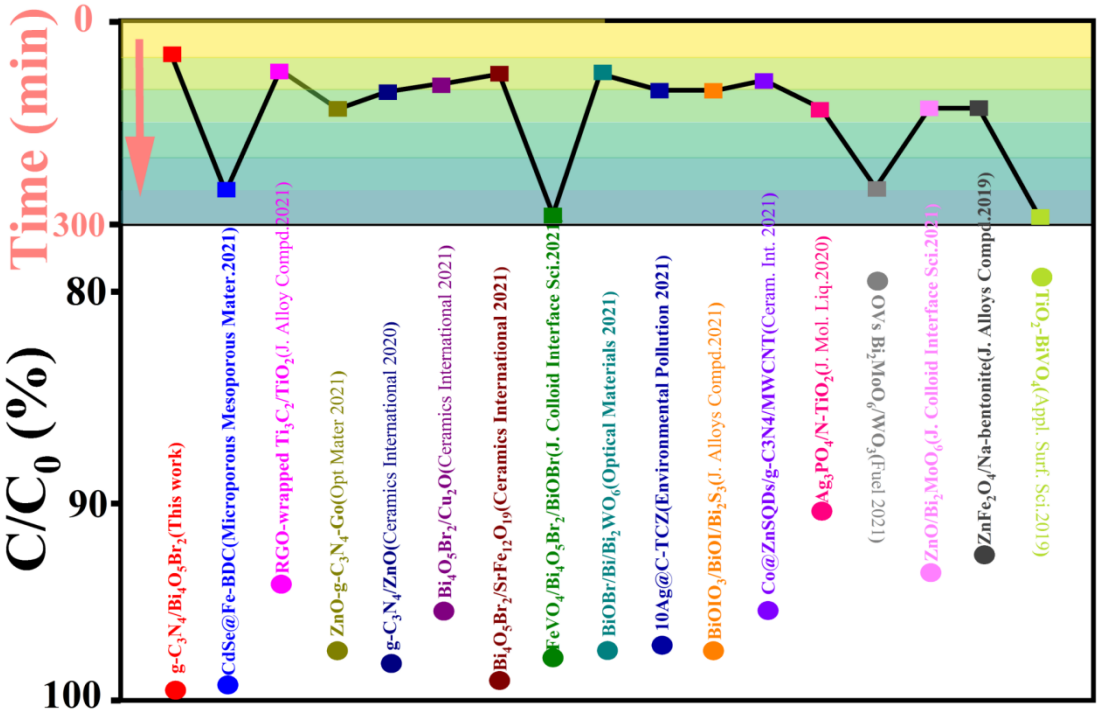

Fig. S10. Comparison of photocatalytic degradation performance using the literature images.

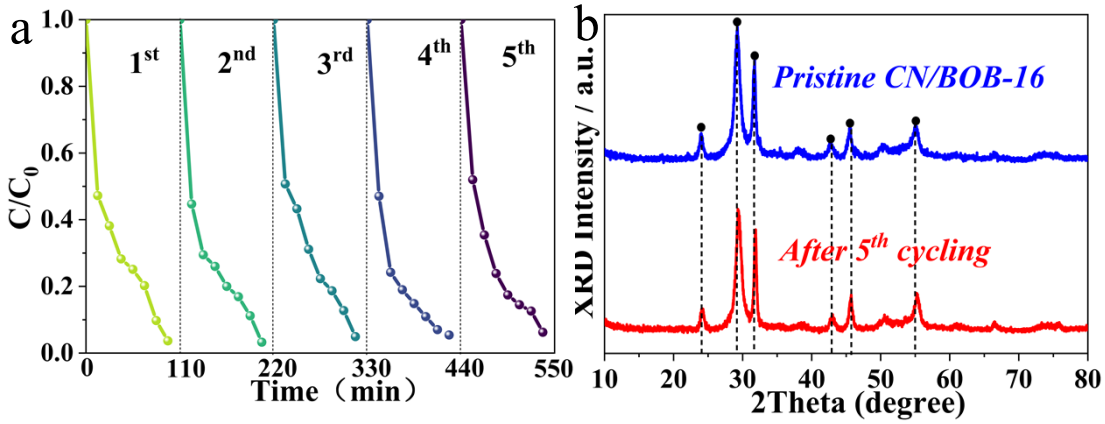

Fig. S11. (a) Recycling ability evaluation for five cycles. **(b)** XRD patterns of the CN/BOB-16 before and after the photocatalytic degradation experiment.

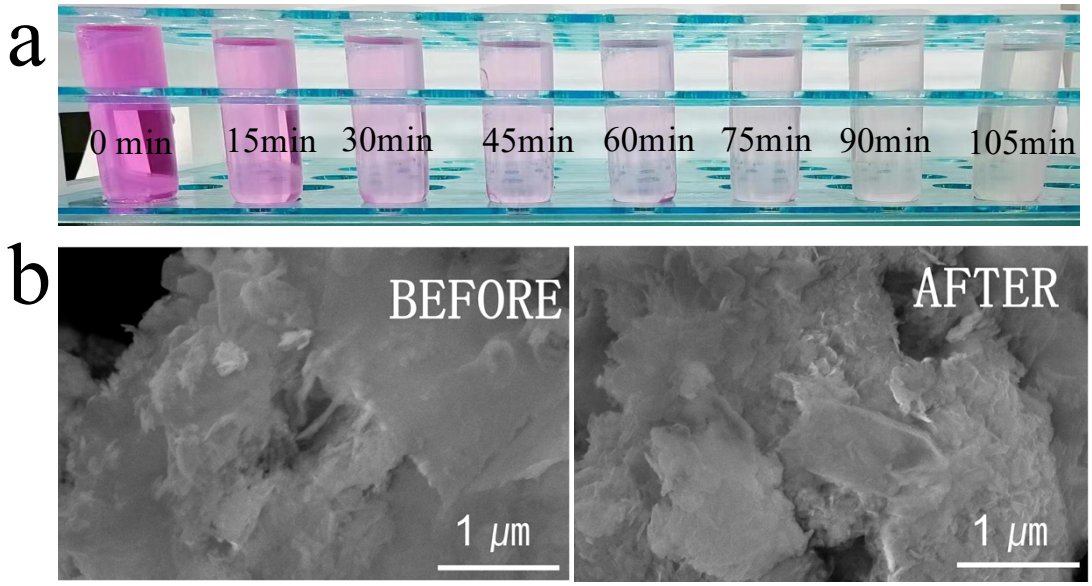

Fig. S12. (a) Photograph of the dye solvents for the 5th cycle. (b) SEM images of the CN/BOB-16 before and after the photocatalytic degradation experiment.

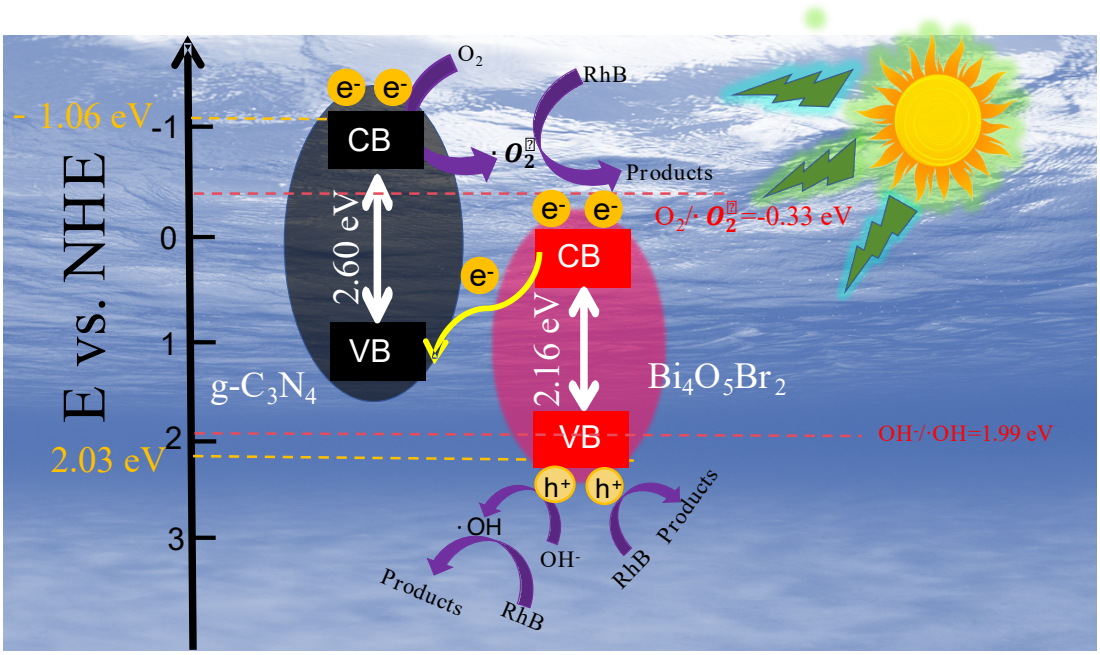

Fig. S13. Mechanism analysis of photocatalytic degradation: Proposed mechanism for the g-C_3N_4/$Bi_4O_5Br_2$ heterojunction.

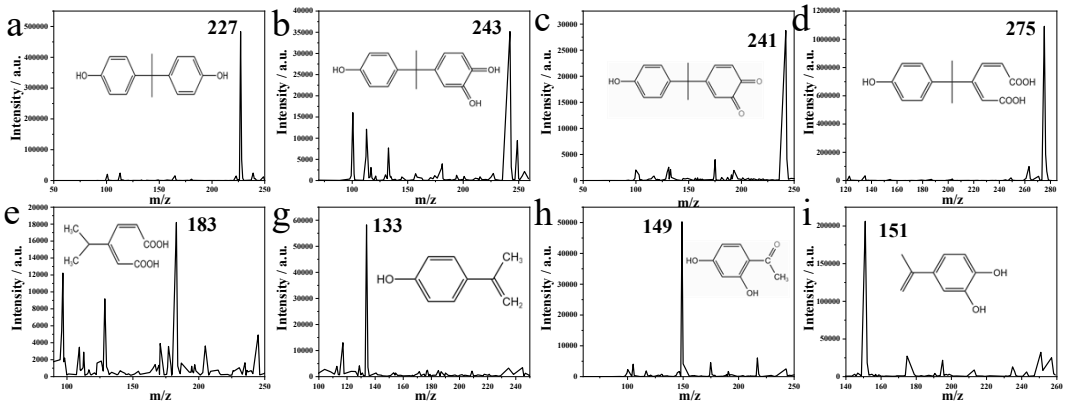

Fig. S14. HPLC-MS analysis conditions of the organic contaminants. (BPA)

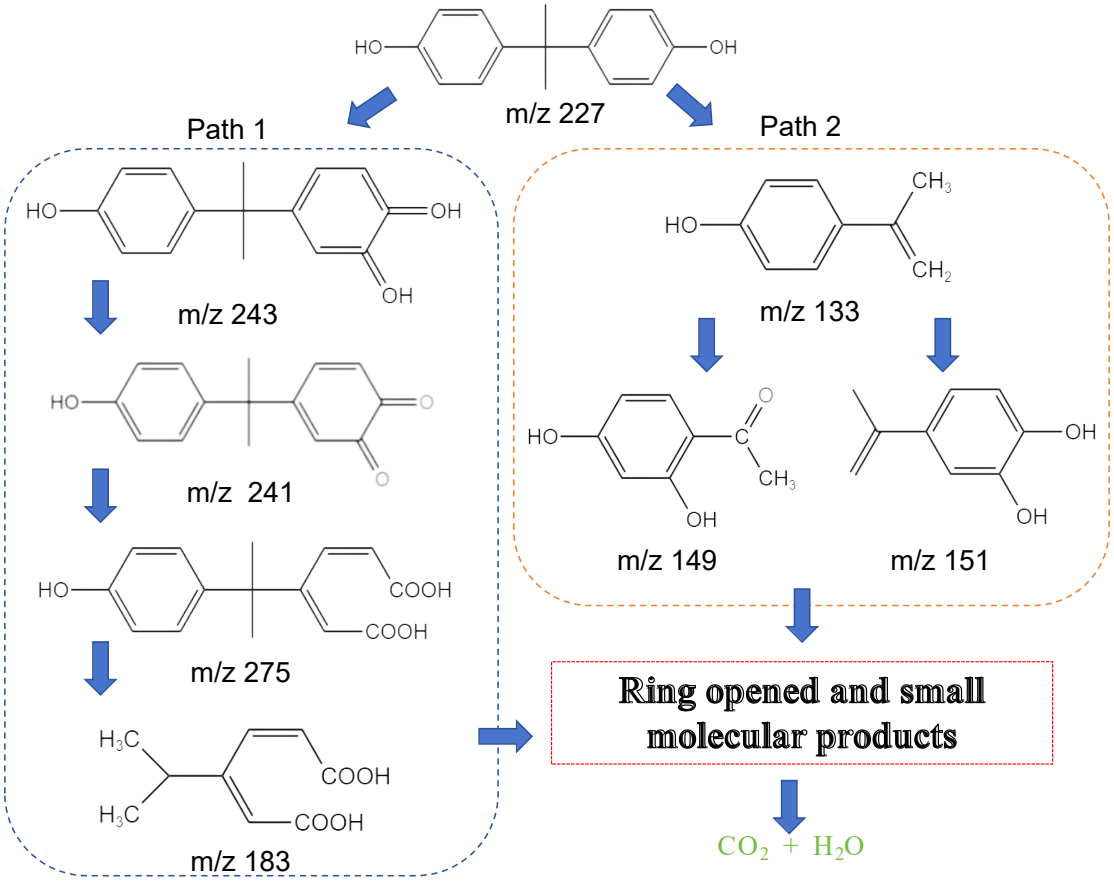

Fig. S15. Possible degradation pathways of BPA. In **Path 1**, hydroxylation was the first step of BPA photoconversion[6, 7], and the aromatic ring was then attacked by $\cdot O_2^-$ to form mono-hydroxylated BPA m/z = 243. Undergone the subsequent dehydration and ring-opening reactions, the corresponding quinone and carboxylic acid compounds m/z =241 and m/z = 275 were produced[8]. Due to the instability of hydroxylated BPA, ring-opening reactions may occur on m/z = 243 and m/z =241 under the attack of the active substance to form the product m/z = 183[9]. In **Path 2**, two phenolic hydroxyl groups in BPA as electron donors increase the electron density of the aromatic ring, which makes the electron-rich CAC connecting the two aromatic rings vulnerable to

the attack of the active species, leading to the form products m/z =133, and m/z =133 further becomes m/z =149 and m/z =151[10]. In the late stage of the reaction, the above-mentioned products are subjected to ring-opening reaction under the continuous attack of the free radicals to generate small molecular products, which are finally converted into CO_2 and H_2O.

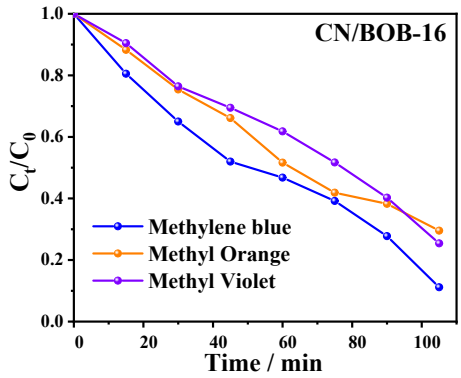

Fig. S16. Degradation properties for the other three dyes: methyl blue (90%), methyl orange (71%), and methyl violet (75%).

Table S1. The fitting parameter for the pseudo-first-order kinetic curve. (RhB)

Samples	CN/BOB-21	CN/BOB-11	CN/BOB-21	CN/BOB-14	CN/BOB-16	CN/BOB-18	CN/BOB-110	CN	BOB
Slopes	0.043± 0.001	0.050± 0.001	0.063± 0.001	0.070± 0.002	0.101± 0.003	0.078± 0.003	0.062± 0.002	0.040 ± 0.002	0.041 ± 0.001
r^2	0.993	0.989	0.993	0.992	0.992	0.988	0.989	0.980	0.987

Table S2. Fitting parameters for the proposed first-order kinetic curve for free radical trapping.

Samples		CN/BOB-16	N_2	KI	IPA		N_2	KI	IPA
Slopes	BPA	0.034± 0.004	0.022 ±0.001	0.006 ±0.001	0.003 ±0.001	RhB	0.011 ±0.001	0.007 ±0.001	0.030 ±0.001
r^2		0.879	0.983	0.976	0.973		0.941	0.997	0.996

Table S3. (BPA and RhB) Total organic carbon removal rate of CN/BOB-16.

Sample(Time)	TOC (mg L^{-1})	Removal Rate
BPA (0)	16.5	-
BPA (80)	3.5	78.8%
RhB (0)	17.8	-

RhB (105)	1.3	92.7%

Table S4. Comparisons of RhB photocatalytic degradation between the prepared composite and some previous reported photocatalysts.

Samples	Light source	RhB Conc(mg/L)	Time(min)	Removal efficiency (%)	Ref
g-C_3N_4/$Bi_4O_5Br_2$	***500 W Xenon lamp***	***10***	***35***	***100***	***This work***
CdSe QDs@ Fe-based metal organic framework	250 W Sodium lamp	50	240	99.8	11
RGO-wrapped Ti_3C_2/TiO_2	300 W Xenon lamp	10	60	94.6	12
ZnO-g-C_3N_4-GO	350 W Xenon lamp	10	120	98	13
g-C_3N_4/ZnO	300 W Xenon lamp	10	90	98.5	14
$Bi_4O_5Br_2/Cu_2O$	300 W Xenon lamp	10	80	96	15
$Bi_4O_5Br_2/SrFe_{12}O_{19}$	300 W Xenon lamp	10	60	99.3	16
$FeVO_4/Bi_4O_5Br_2$/BiOBr	50 W LED lamp	10	360	98.2	17
BiOBr/Bi/Bi_2WO_6	350 W Xe lamp	10	60	98	18
Ag NPs decorated C-$TiO_2/Cd_{0.5}Zn_{0.5}S$	500 W Xe lamp	7	90	97.6	19
$BiOIO_3$/BiOI/Bi_2S_3	500 W Xe lamp	10	90	98	20
Co@ZnSQDs/g-C_3N_4 /MWCNT	halogen lamp 500 W	10	75	96	21
Ag_3PO_4/N-TiO_2	150W Xe lamp	10	120	91	22
OVs Bi_2MoO_6/WO_3	300 W Xe lamp	10	240	80	23
ZnO/Bi_2MoO_6	15 W Panasonic cool daylight lamp	10	120	94	24
$ZnFe_2O_4$/Na-bentonite	350 W Xenon lamp	10	120	93	25

TiO_2-$BiVO_4$	300 Xe lamp	10	300	79.3	[26]

References

1. Chen, X.; Zhang, J.; Zeng, J. H.; Shi, Y. X.; Huang, G. Z.; Zhang, L. L.; Wang, H. B.; Kong, Z.; Xi, J. H.; Ji, Z. G., Novel 3D/2D heterojunction photocatalysts constructed by three-dimensional In2S3 dandelions and ultrathin hexagonal SnS2 nanosheets with excellent photocatalytic and photoelectrochemical activities. *Applied Surface Science* **2019,** *463*, 693-703.

2. Hu, M.; Yan, A. H.; Wang, X. Y.; Huang, F.; Cui, Q. P.; Li, F.; Huang, J., Hydrothermal method to prepare Ce-doped BiOBr nanoplates with enhanced carrier transfer and photocatalytic activity. *Materials Research Bulletin* **2019,** *116*, 89-97.

3. Jiao, H. P.; Yu, X.; Liu, Z. Q.; Kuang, P. Y.; Zhang, Y. M., One-pot synthesis of heterostructured Bi2S3/BiOBr microspheres with highly efficient visible light photocatalytic performance. *Rsc Advances* **2015,** *5* (21), 16239-16249.

4. Xu, T. H.; Zou, R. J.; Lei, X. F.; Qi, X. M.; Wu, Q.; Yao, W. F.; Xu, Q. J., New and stable g-C3N4/HAp composites as highly efficient photocatalysts for tetracycline fast degradation. *Applied Catalysis B-Environmental* **2019,** *245*, 662-671.

5. Zhao, Y. J.; Liu, Y.; Cao, J. J.; Wang, H.; Shao, M. W.; Huang, H.; Liu, Y.; Kang, Z. H., Efficient production of H2O2 via two-channel pathway over ZIF-8/C3N4 composite photocatalyst without any sacrificial agent. *Applied Catalysis B-Environmental* **2020,** *278*.

6. Wu, Z.; Shen, J.; Ma, N.; Li, Z.; Wu, M.; Xu, D.; Zhang, S.; Feng, W.; Zhu, Y., Bi4O5Br2 nanosheets with vertical aligned facets for efficient visible-light-driven photodegradation of BPA. *Applied Catalysis B: Environmental* **2021,** *286*, 119937.

7. Zhang, H.; Zheng, Y.; Wang, X. C.; Zhang, Q.; Dzakpasu, M., Photochemical behavior of constructed wetlands-derived dissolved organic matter and its effects on Bisphenol A photodegradation in secondary treated wastewater. *Science of The Total Environment* **2022,** *845*, 157300.

8. Lai, J.; Jiang, X.; Zhao, M.; Cui, S.; Yang, J.; Li, Y., Thickness-dependent layered BiOIO3 modified with carbon quantum dots for photodegradation of bisphenol A: Mechanism, pathways and DFT calculation. *Applied Catalysis B: Environmental* **2021,** *298*, 120622.

9. Xu, L.; Yang, L.; Johansson, E. M. J.; Wang, Y.; Jin, P., Photocatalytic activity and mechanism of bisphenol a removal over TiO2−x/rGO nanocomposite driven by visible light. *Chemical Engineering Journal* **2018,** *350*, 1043-1055.

10. Takdastan, A.; Kakavandi, B.; Azizi, M.; Golshan, M., Efficient activation of peroxymonosulfate by using ferroferric oxide supported on carbon/UV/US system: A new approach into catalytic degradation of bisphenol A. *Chemical Engineering Journal* **2018,** *331*, 729-743.

11. Zhang, Y.; Li, G.; Guo, Q. Y., CdSe QDs@ Fe-based metal organic framework composites for improved photocatalytic RhB degradation under visible light. *Microporous Mesoporous Mat.* **2021,** *324*, 10.

12. Xu, C.; Yang, F.; Deng, B. J.; Che, S.; Yang, W.; Zhang, G.; Sun, Y. K.; Li, Y. F., RGO-wrapped Ti3C2/TiO2 nanowires as a highly efficient photocatalyst for simultaneous reduction of Cr(VI) and degradation of RhB under visible light irradiation. *Journal of Alloys and Compounds* **2021,** *874*.

13. Zhang, J. Q.; Li, J.; Liu, X. Y., Ternary nanocomposite ZnO-g-C(3)N4-Go for enhanced photocatalytic degradation of RhB. *Optical Materials* **2021,** *119*.

14. Zhong, Q. D.; Lan, H. Y.; Zhang, M. M.; Zhu, H.; Bu, M., Preparation of heterostructure g-C3N4/ZnO nanorods for high photocatalytic activity on different pollutants (MB, RhB, Cr(VI) and eosin). *Ceramics International* **2020,** *46* (8), 12192-12199.

15. Liu, G.; Wang, Y.; Sun, Y. H.; He, J. X., Synthesis of hollow structured Bi4O5Br2/Cu2O P-N heterojunctions with large surface area for enhanced photocatalytic performance towards the degradation of organic dyes. *Ceramics International* **2021,** *47* (20), 28650-28658.
16. Wang, H. L.; Xu, L. J.; Wu, X.; Zhang, M. J., Eco-friendly synthesis of a novel magnetic Bi4O5Br2/SrFe12O19 nanocomposite with excellent photocatalytic activity and recyclable performance. *Ceramics International* **2021,** *47* (6), 8300-8307.
17. Chachvalvutikul, A.; Luangwanta, T.; Kaowphong, S., Double Z-scheme FeVO4/Bi4O5Br2/BiOBr ternary heterojunction photocatalyst for simultaneous photocatalytic removal of hexavalent chromium and rhodamine B. *Journal of Colloid and Interface Science* **2021,** *603*, 738-757.
18. Chen, X. L.; Zhao, B. X.; Ma, J. X.; Liu, L. X.; Luo, H. D.; Wang, W. J., The BiOBr/Bi/Bi2WO6 photocatalyst with SPR effect and Z-scheme heterojunction synergistically degraded RhB under visible light. *Optical Materials* **2021,** *122*.
19. Wang, Y. H.; Kang, C. L.; Li, X. Y.; Hu, Q.; Wang, C., Ag NPs decorated C-TiO2/Cd0.5Zn0.5S Z-scheme heterojunction for simultaneous RhB degradation and Cr(VI) reduction. *Environmental Pollution* **2021,** *286*.
20. Lu, M. L.; Xiao, X. Y.; Zeng, G. C., Bi2S3 nanorods and BiOI nanosheets co-modified BiOIO3 nanosheets: An efficient vis-light response photocatalysts for RhB degradation. *Journal of Alloys and Compounds* **2021,** *885*.
21. Danish, M.; Muneer, M., Facile synthesis of highly efficient Co@ZnSQDs/g-C3N4/MWCNT nanocomposites and their photocatalytic potential for the degradation of RhB dye: Efficiency, degradation kinetics, and mechanism pathway. *Ceramics International* **2021,** *47* (9), 13043-13056.
22. Khalid, N. R.; Mazia, U.; Tahir, M. B.; Niaz, N. A.; Javid, M. A., Photocatalytic degradation of RhB from an aqueous solution using Ag3PO4/N-TiO2 heterostructure. *Journal of Molecular Liquids* **2020,** *313*.
23. Zhang, Z. S.; Zhao, C. X.; Lin, S. L.; Li, H.; Feng, Y. L.; Gao, X., Oxygen vacancy modified Bi2MoO6/WO3 electrode with enhanced photoelectrocatalytic degradation activity toward RhB. *Fuel* **2021,** *285*.
24. Chankhanittha, T.; Nanan, S., Visible-light-driven photocatalytic degradation of ofloxacin (OFL) antibiotic and Rhodamine B (RhB) dye by solvothermally grown ZnO/Bi2MoO6 heterojunction. *Journal of Colloid and Interface Science* **2021,** *582*, 412-427.
25. Guo, Y. Q.; Guo, Y. D.; Tang, D. D.; Liu, Y. Y.; Wang, X. G.; Li, P.; Wang, G. H., Sol-gel synthesis of new ZnFe2O4/Na-bentonite composites for simultaneous oxidation of RhB and reduction of Cr(VI) under visible light irradiation. *Journal of Alloys and Compounds* **2019,** *781*, 1101-1109.
26. Wang, Y. Q.; Lu, N.; Luo, M.; Fan, L. Y.; Zhao, K.; Qu, J.; Guan, J. N.; Yuan, X., Enhancement mechanism of fiddlehead-shaped TiO2-BiVO4 type II heterojunction in SPEC towards RhB degradation and detoxification. *Applied Surface Science* **2019,** *463*, 234-243.